J Membrane Biol (2016) 249:181–196
DOI 10.1007/s00232-015-9859-9

Topography of the TH5 Segment in the Diphtheria Toxin T-Domain Channel

Paul K. Kienker[1] · Zhengyan Wu[1,3] · Alan Finkelstein[1,2]

Received: 28 September 2015 / Accepted: 18 November 2015 / Published online: 8 December 2015
© Springer Science+Business Media New York 2015

Abstract The translocation domain (T-domain) of diphtheria toxin contains 10 α helices in the aqueous crystal structure. Upon exposure to a planar lipid bilayer under acidic conditions, it inserts to form a channel and transport the attached amino-terminal catalytic domain across the membrane. The TH5, TH8, and TH9 helices form transmembrane segments in the open-channel state, with TH1–TH4 translocated across the membrane. The TH6–TH7 segment also inserts to form a constriction that occupies only a small portion of the total channel length. Here, we have examined the TH5 segment in more detail, using the substituted-cysteine accessibility method. We constructed a series of 23 mutant T-domains with single cysteine residues at positions in and near TH5, monitored their channel formation in planar lipid bilayers, and probed for an effect of thiol-specific reagents added to the solutions on either side of the membrane. For 15 of the mutants, the reagent caused a decrease in single-channel conductance, indicating that the introduced cysteine residue was exposed within the channel lumen. We also found that reaction caused large changes in ionic selectivity for some mutant channels. We determined whether reaction occurred in the open state or in the brief flicker-closed state of the channel. Finally, we compared the reaction rates from either side of the membrane. Our experiments are consistent with the hypotheses that the TH5 helix has a transmembrane orientation and remains helical in the open-channel state; they also indicate that the middle of the helix is aligned with the constriction in the channel.

Keywords Bacterial toxins · Ion-conducting channels · Kinetics · Lipid bilayers · Sulfhydryl reagents

Abbreviations

C-domain	Catalytic domain of DT
DT	Diphtheria toxin
DTT	Dithiothreitol
His_6-tag	Hexahistidine tag
I–V	Current–voltage
MTS	Methanethiosulfonate
MTS-ACE	[2-(Aminocarbonyl)ethyl] MTS
MTS-ET	[2-(Trimethylammonium)ethyl] MTS bromide
SCAM	Substituted-cysteine accessibility method
T-domain	Translocation domain of DT

Introduction

Diphtheria toxin (DT) is a water-soluble protein with three structural domains (Bennett et al. 1994), each of which plays a key functional role in the intoxication of the target cell. [See Murphy (2011) for a review.] The carboxy-terminal receptor-binding domain binds to a receptor on the cell surface. Following proteolytic nicking, endocytosis, and the acidification of the endosome, the central

✉ Paul K. Kienker
kienker@outlook.com

[1] Department of Physiology and Biophysics, Albert Einstein College of Medicine, 1300 Morris Park Avenue, Bronx, NY 10461, USA

[2] Department of Neuroscience, Albert Einstein College of Medicine, 1300 Morris Park Avenue, Bronx, NY 10461, USA

[3] Present Address: Key Laboratory of Ion Beam Bioengineering, Hefei Institutes of Physical Science, Chinese Academy of Sciences, Hefei 230031, Anhui, China

translocation or transmembrane domain (T-domain) changes its conformation to insert into the endosomal membrane and facilitate the translocation of the amino-terminal catalytic domain (C-domain) across the membrane to the cytosol, where reduction of a disulfide bond frees the C-domain from the T-domain. Once it has been delivered to the cytosol, the C-domain acts as an enzyme to ADP-ribosylate a specific post-translationally modified histidine residue, known as diphthamide, in elongation factor 2, thereby blocking protein synthesis and leading to cell death.

Whole DT and fragments containing the T-domain are able to form channels in liposomes and in planar lipid bilayers when the solution on the *cis* side (the side to which DT is added) is acidic (pH $\sim$ 5) (Donovan et al. 1981; Kagan et al. 1981). It is widely believed that channel formation by the T-domain is necessary for translocation of the C-domain, although the precise connection between the two has not been determined (Murphy 2011). In the aqueous crystal structure of DT, the T-domain consists of 10 α helices, designated TH1–TH5, TH5′, and TH6–TH9 (Bennett et al. 1994). Although early studies emphasized the importance of the TH8–TH9 hairpin in channel formation (Silverman et al. 1994; Oh et al. 1996; Huynh et al. 1997; Oh et al. 1999b), it was subsequently shown that the TH5 segment also spans the membrane in the open-channel state, with TH1–TH4 (and the C-domain, if present) translocated across the membrane to the opposite, *trans*, side (Fig. 1) (Senzel et al. 1998; Oh et al. 1999a; Senzel et al. 2000). Spectroscopic studies (Rosconi and London 2002; Rosconi et al. 2004; Zhao and London 2005; Lai et al. 2008; Wang and London 2009) have shown that DT can also assume other conformations in the membrane, but it is not clear whether these conformations correspond to open states of the channel, particularly since these are states in which the amino terminus has not been translocated. A study using neutron reflectometry and solid-state NMR spectroscopy identified a pretranslocation state; although the water content within the plane of the membrane was enhanced in this state, it is not clear that it was actually an ion-conducting state (Chenal et al. 2009). More recently, we have shown that the TH6–TH7 segment lines the channel, and forms a sort of open hairpin that dips into the membrane from the *cis* side, but does not span the membrane (Fig. 1) (Kienker et al. 2015). Moreover, the TH6–TH7 segment appears to form a constriction in the channel, with residues in TH8 lying on either side of the constriction (Kienker et al. 2015).

To complete this series of studies, we now examine the TH5 segment, to see which of its residues line the open channel, and to see how they are located relative to the channel constriction. We do this primarily by measuring the accessibility of substituted-cysteine residues in TH5 to sulfhydryl-specific reagents in the *cis* or *trans* solution, similar to our approach in the TH6–TH7 study (Kienker et al. 2015). This will allow us to determine the alignment of TH5 relative to the other channel-lining segments.

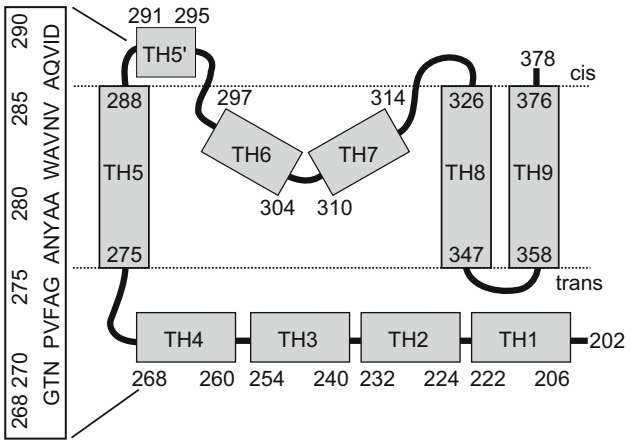

Fig. 1 Topological model of the T-domain channel, based on the work of Senzel et al. (2000) and Kienker et al. (2015). The ten shaded rectangles represent α-helical segments (TH1 through TH9) as defined in the aqueous crystal structure, with the *numbers* at each end indicating the residues at each end of the helix (Bennett et al. 1994). The residues at the amino- and carboxy-terminal ends of our construct (not counting the His_6-tag) are also indicated. The *horizontal dotted lines* indicate the approximate boundaries of the lipid bilayer's hydrocarbon region. The amino-acid sequence of residues 268–290, the segment that we are studying here, is given at the *left*

Materials and Methods

Mutagenesis and Protein Preparation

Cloning, expression, and protein purification of the T-domain constructs were performed as described previously (Zhan et al. 1995), with induction at 30 °C. Site-directed mutagenesis was done using the QuikChange site-directed mutagenesis kit (Agilent Technologies, Santa Clara, CA). The wild-type T-domain (residues 202–378 of DT) contains no cysteine residues. The expressed proteins contained an amino-terminal hexahistidine tag (His_6-tag) with the sequence Gly-Ser-Ser-$(His)_6$-Ser–Ser-Gly-Leu-Val-Pro-Arg-Gly-Ser-His-Met. [As shown by Senzel et al. (1998), the amino-terminal methionine encoded in the plasmid construct is removed during expression.) As noted before, the His_6-tag blocks the channel at *cis* negative voltages (Senzel et al. 1998). For many experiments, we did not want this behavior, so we removed the His_6-tag by thrombin cleavage, leaving the four residues Gly-Ser-His-Met at the amino terminus. With or without the His_6-tag, we use the standard residue numbers derived for whole DT

(Greenfield et al. 1983). In the study of Senzel et al. (2000), residues 267 and 291 were located on the *trans* and *cis* sides, respectively, so here we performed cysteine mutagenesis at the intervening residues 268–290, from the end of TH4 through the TH5–TH5′ loop (Bennett et al. 1994).

Mutant proteins at concentrations of ~1 mg/ml were stored at −80 °C in 20 mM Tris, pH 8.0, with 2 mM dithiothreitol (DTT), and retained their channel-forming activity for at least 10 years. Before use, a thawed sample was incubated with 10 mM DTT for 5 min at room temperature to ensure reduction of the cysteine sulfhydryl group. DTT solutions were prepared daily from 1 M stock, which was stored at −20 °C.

Planar Bilayer Experiments

Planar phospholipid bilayers were formed by the Montal–Mueller technique (Montal 1974) across a small hole (typically ~100-μm diameter) in a partition separating two compartments, designated *cis* and *trans*, with T-domain always added to the *cis* compartment. Typically, ~1 μg of protein was added to produce macroscopic channel activity. As previously described (Kienker et al. 2015), two types of chamber were used, with the compartments separated either by a Teflon partition or by the side of a polystyrene "cup." The compartment volumes ranged from 0.5 to 1.5 ml. The chambers were pretreated with solutions of squalene and asolectin as described. The bathing solution was generally 1 M KCl, 2 mM $CaCl_2$, 1 mM EDTA, and an appropriate buffer: typically 20 mM malic acid, pH 5.3 in the *cis* compartment and 20 mM HEPES, pH 7.2 in the *trans* compartment. In experiments when the *cis* pH was to be raised after channel formation, the *cis*-side buffer was typically 5 mM MES, pH 5.3, and concentrated HEPES solution was added to raise the *cis* pH. We found that a *cis* pH of 6.2 gave a reasonable compromise between the speed of reaction with methanethiosulfonate (MTS) compounds (faster at higher pH) and the stability of the channel activity (more stable at lower *cis* pH). Selectivity experiments used 1 M KCl (*cis*) versus 0.1 M KCl (*trans*), along with the other ingredients listed above.

Voltage-clamp recordings were performed with three different setups, as previously described (Kienker et al. 2015), with most experiments using a BC-525C Bilayer Clamp amplifier (Warner Instruments, Hamden, CT) and an NI USB-6211 A/D converter (National Instruments, Austin, TX). The program Igor Pro (6.3.7.2) with the NIDAQ Tools MX package (1.0.5.4) (WaveMetrics, Lake Oswego, OR) was used for data acquisition and analysis. The voltage is defined as the potential of the *cis* compartment, relative to the *trans*-side ground. The current signal was low-pass filtered with an LPF-8 Bessel filter (Warner Instruments), with cutoff frequency typically in the range 5–30 Hz. For the experiments to identify the conductance state in which reaction occurred, we used cup chambers with a smaller hole (~30-μm diameter) to reduce the noise, and filtered at 1000 Hz, as described (Kienker et al. 2015).

The MTS reagents used were [2-(trimethylammonium)ethyl] MTS bromide (MTS-ET) (Biotium, Hayward, CA) and [2-(aminocarbonyl)ethyl] MTS (MTS-ACE) (Toronto Research Chemicals, Toronto, ON, Canada). Stock solutions in water of MTS-ET (2–200 mg/ml) and MTS-ACE (20–40 mg/ml) were stored at −20 °C.

Data Analysis

To determine MTS reaction rates from macroscopic experiments, we followed our previously described procedure (Kienker et al. 2015), which is summarized below. Typically, a reaction beginning at time $t = 0$ caused an approximately exponential decay in the current from I_0 to a new level I_∞; that is, $I(t) = I_\infty + (I_0 - I_\infty)\ \exp(-k_1 t)$. However, there was sometimes a slower component of decay, attributable to channel gating after reaction. We provisionally assumed that at least the initial part of the current decay had exponential kinetics corresponding to the reaction rate. Then the pseudo-first-order rate constant, k_1, can be estimated as

$$k_1 = \frac{\left[\left(-\frac{dI}{dt}\right)/I_0\right]}{(I_0 - I_\infty)/I_0}, \tag{1a}$$

with dI/dt evaluated at $t = 0$. The numerator is the magnitude of the initial slope of the normalized current trace, and the denominator is the fractional decrease in current over the course of the reaction. (Equivalently, conductances may be used in place of currents.) We used the same value of the denominator for calculating *cis*- and *trans*-side reaction rates. The second-order rate constant, k, presented in the tables was calculated from the formula

$$k = k_1/[\mathrm{MTS}]. \tag{1b}$$

If the *cis* solution is perfused to remove excess T-domain that has not bound to the membrane, there ensues a slow decrease in current ($k_1 \sim 0.003\ s^{-1}$) that we attribute to "washout" of channels from the membrane (Kienker et al. 2015). *Cis* MTS that reacts with and inactivates T-domain in the *cis* solution could produce a similar effect. Thus, we do not consider such a slow effect of *cis* MTS to be reliable evidence of reaction with channels in the membrane.

To describe the relative rates of reaction with *cis* and *trans* reagent, we found it useful to define a relative accessibility value,

$$f = 1/(1 + k_{cis}/k_{trans}). \tag{2a}$$

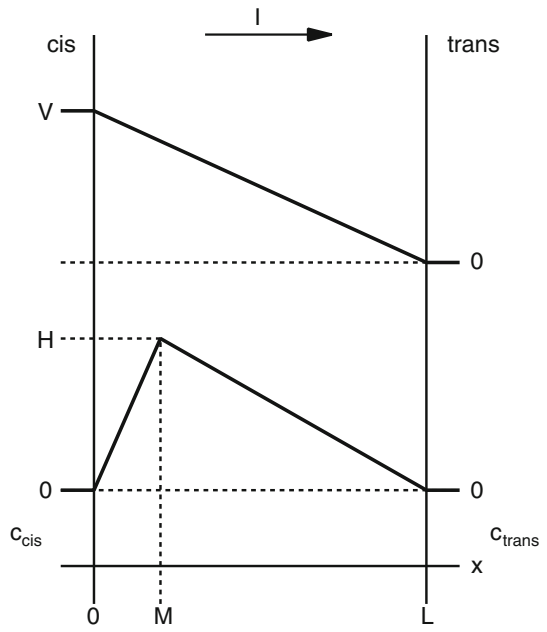

Fig. 2 Potentials used in the Nernst–Planck model. See text for details

This value can range from $f = 0$ for a cysteine that reacts only with *cis* reagent to $f = 1$ for a cysteine that reacts only with *trans* reagent. We approximate the standard deviation of f with the formula

$$\sigma_f \approx \frac{\left(\mu_c^2\sigma_t^2 + \mu_t^2\sigma_c^2\right)^{0.5}}{\left(\mu_c + \mu_t\right)^2}, \tag{2b}$$

where μ_c and σ_c are the mean and standard deviation, respectively, of k_{cis}, and likewise for μ_t, σ_t, and k_{trans}.

$H = 0$ for the unreacted channel and $H > 0$ for the reacted channel. (The assumption of a constant field in the unreacted channel was made for simplicity, as it is consistent with the linear *I–V* curves observed.) The *cis* and *trans* interfaces are at $x = 0$ and $x = L$, respectively. Thus,

$$\psi(x) = V\left(1 - \frac{x}{L}\right) + \left\{\begin{array}{ll} \dfrac{Hx}{M}, & 0 \le x \le M \\ \dfrac{H(L-x)}{(L-M)}, & M \le x \le L \end{array}\right\}. \tag{3}$$

The Nernst–Planck equation gives the current, I_S, carried by a given permeant ionic species, S, as

$$I_S = -z_S F A D_S \left(\frac{dc_S}{dx} + \frac{z_S F c_S}{RT}\frac{d\psi}{dx}\right), \tag{4}$$

where S has valence z_S, concentration $c_S(x)$, and diffusion coefficient D_S, while A, F, R, and T are the cross-sectional area of the channel, the Faraday constant, the gas constant, and the absolute temperature, respectively. For simplicity, we take A and D_S as constants, even though we actually think that $A(x)$ is not constant. We also introduce partition coefficients, β_S, to account for the ionic selectivity of the unreacted channel. Assuming a monovalent: monovalent salt solution with bulk concentrations c_{cis} and c_{trans}, the ionic concentrations "just inside" the channel are $\beta_S c_{cis}$ at $x = 0$ and $\beta_S c_{trans}$ at $x = L$. Equation 4 has solution

$$I_S = z_S F A D_S \beta_S \frac{\left(c_{cis} e^{z_S F V/RT} - c_{trans}\right)}{\int_0^L e^{z_S F \psi(x)/RT} dx} \tag{5}$$

(Hille 2001). Substituting $\psi(x)$ from Eq. 3 into Eq. 5 and evaluating the integral gives the formula

$$I_S = \frac{g_S (H - V\phi)(H + V - V\phi)\left(e^{z_S FV/RT} - c_{trans}/c_{cis}\right)}{\left[H e^{z_S F(H+V-V\phi)/RT} - \phi(H + V - V\phi)e^{z_S FV/RT} - (1-\phi)(H - V\phi)\right]}, \tag{6}$$

Electrodiffusion Model

We used a one-dimensional Nernst–Planck electrodiffusion model to fit single-channel current–voltage (*I–V*) relations of T-domain mutant channels before and after reaction with MTS-ET, with the aim of relating the shape of the *I–V* curve to the position of the reactive site. The electrical potential, ψ, as a function of the position along the channel axis, x, was assumed to be the sum of two components: a linear (constant field) term arising from the applied voltage, V, and a triangular potential with peak height H at position $x = M$ arising from the positive charge introduced at this position by reaction with MTS-ET (Fig. 2). That is,

where we have defined $\phi \equiv M/L$, the fractional distance of the triangular potential's peak from the *cis* side, and combined the scaling factors as $g_S \equiv z_S^2 F^2 A D_S \beta_S c_{cis}/RTL$. (We do not have enough information about the channel to set all the component factors individually.)

For KCl solutions, the total current is $I = I_K + I_{Cl}$. (Although I_{Cl} could be neglected for the wild-type channel, it becomes significant for some mutants upon reaction with MTS-ET.) For fitting the data, we found it desirable to use scaling factor $g \equiv g_K + g_{Cl}$ and a conventionally defined permeability ratio $P_{K/Cl} = g_K/g_{Cl}$ as model parameters, along with ϕ and H. Thus, $g_K = g\ P_{K/Cl}/(1 + P_{K/Cl})$ and $g_{Cl} = g/(1 + P_{K/Cl})$.

Our standard fitting procedure was to first choose $P_{K/Cl}$ to match the reversal potential of wild-type T-domain channels in KCl-gradient experiments, using the Goldman–Hodgkin–Katz equation (Hille 2001). Then, for each mutant, g was determined by fitting $I(V)$ to the unreacted channel's I–V data, with H fixed to zero. (In this case, the formula simplifies to $I = gV$ for symmetric salt solutions.) With this value of g fixed, $I(V)$ was fitted to the reacted channel's I–V data to obtain ϕ and H. (By using the same value of g for unreacted and reacted channels, we are supposing, in essence, that the effect of MTS-ET reaction is purely electrostatic, with no steric effect.)

Results

Initial Screening of Mutant T-Domain Channels

We prepared a series of mutant T-domain proteins with a single cysteine residue introduced from residues 268–290, a segment identified as membrane-spanning by Senzel et al. (2000). The segment is uncharged except for Asp-290, and includes one residue at the end of TH4, the TH4–TH5 loop, TH5, and the TH5–TH5′ loop. [For convenience, we sometimes refer to this entire segment as "TH5," but only residues 275–288 are actually in the TH5 helix in the aqueous crystal structure (Bennett et al. 1994).] All mutants showed relatively normal macroscopic channel activity in planar bilayers. Most of the mutant channels had normal single-channel conductance [35–50 pS in 1 M KCl, pH 5.3 (*cis*): 7.2 (*trans*)] compared with that of wild-type T-domain channels (≈40 pS; Huynh et al. 1997), but N277C, W281C, and Q287C channels had lower conductances (16, 27, and 22 pS, respectively). It is notable that D290C mutant channels had a normal single-channel conductance, despite the substitution of a negative charge with a neutral group; this suggests that residue 290 may not line the channel.

As previously reported, T-domain with an amino-terminal His_6-tag forms channels that show rapid blocking at negative voltages and rapid unblocking at positive voltages; this is due to the His_6-tag being translocated across the membrane during channel formation and then blocking the channel from the *trans* side (Senzel et al. 1998). We verified that all of our mutants showed His_6-tag blocking with the normal voltage polarity, indicating normal translocation of the amino terminus.

Effects of MTS-ET on Macroscopic Conductance

We applied the substituted-cysteine accessibility method (SCAM) (Karlin and Akabas 1998) to the TH5 segment of T-domain, using the positively charged, sulfhydryl-specific reagent MTS-ET to probe for an effect on channel properties. Although our principal criterion for identifying a channel-lining residue is a change in single-channel conductance upon reaction, macroscopic experiments are more useful for determining the rate of reaction. Figure 3a shows an example of a mutant (N277C) that reacted more rapidly from the *trans* side and Fig. 3b shows one (W281C) that reacted more rapidly from the *cis* side. Of the 23 mutants tested, 15 showed an effect of *cis* or *trans* MTS-ET on the macroscopic conductance (Table 1). (Mutants that showed only a slow effect of *cis* MTS-ET are excluded, as the effect could be due to washout of channels from the membrane following reaction in the *cis* solution.) It can be seen that mutants from G268C to Y278C reacted faster with *trans* than with *cis* MTS-ET, whereas mutants from A280C to V288C reacted faster with *cis* than with *trans* MTS-ET.

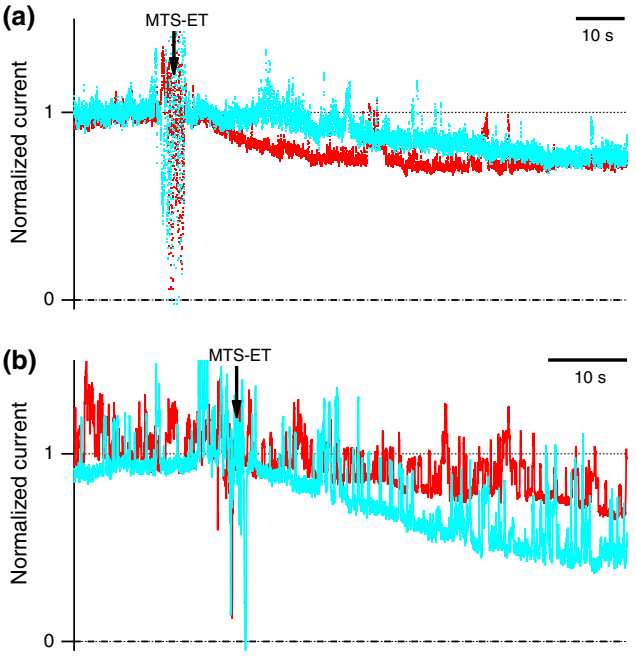

Fig. 3 Comparison of *cis*- and *trans*-side reaction rates of MTS-ET with T-domain TH5 segment mutants N277C and W281C. Records from two experiments are superimposed in each panel, showing normalized current against time. In each case, mutant T-domain protein was added to the *cis* solution several minutes before the start of the record, and the channel activity was allowed to stabilize. **a** N277C with 0.1 mM MTS-ET. **b** W281C with 0.7 mM MTS-ET. In each panel, MTS-ET was added at the *arrow* to either the *cis* (*cyan trace*) or *trans* (*red trace*) compartment, causing a decay to a lower current level. It can be seen that for N277C channels, reaction with *trans* MTS-ET was faster than reaction with *cis* MTS-ET. The reverse was true for W281C channels, which reacted more quickly with *cis* than with *trans* MTS-ET. For both panels, the solutions were 1 M KCl, 2 mM $CaCl_2$, 1 mM EDTA, with 20 mM malic acid, pH 5.3 in the *cis* compartment and 20 mM HEPES, pH 7.2 in the *trans* compartment. The holding potential was 30 mV in each case

Table 1 Percent conductance change upon reaction and rates of reaction with MTS-ET of mutant channels in macroscopic experiments

Mutant	*cis* pH	mV	MTS-ET side	Macroscopic conductance change (%)	k_{cis} (M^{-1} s^{-1})	k_{trans} (M^{-1} s^{-1})	Relative accessibility value *f*
G268C	5.3	30	*cis* and *trans*	−16 ± 2 ($n = 5$)	106 ± 100 ($n = 2$)	1570 ± 26 ($n = 2$)	0.94 ± 0.06
T269C	5.3	20-60	*trans*	−9 ± 2 ($n = 3$)	NE ($n = 3$)	330 ± 56 ($n = 2$)	1
V272C	5.3	30	*cis* and *trans*	−18 ± 2 ($n = 2$)	14 ± 1 ($n = 2$)	39 ± 7 ($n = 2$)	0.73 ± 0.04
A274C	5.3	30	*cis* and *trans*	−14 ± 3 ($n = 11$)	257 ± 121 ($n = 4$)	716 ± 685 ($n = 5$)	0.74 ± 0.21
G275C	5.3	10-50	*trans*	−56 ± 15 ($n = 6$)[a]	NE ($n = 4$)	11 ± 10 ($n = 6$)	1
A276C	5.3	30	*cis* and *trans*	−78 ± 19 ($n = 4$)[a]	5 ± 3 ($n = 2$)	8.6 ± 0.6 ($n = 2$)	0.62 ± 0.14[a]
N277C	5.3	30	*cis* and *trans*	−40 ± 7 ($n = 11$)	80 ± 38 ($n = 4$)	128 ± 51 ($n = 5$)	0.62 ± 0.15
Y278C	5.3	30	*trans*	−44 ± 2 ($n = 2$)	0.8 ± 0.2 ($n = 2$)	1.8 ± 0.4 ($n = 4$)	0.68 ± 0.07
A280C	6.2	30	*cis* and *trans*	−94 ± 3 ($n = 4$)[a]	24 ± 5 ($n = 3$)	6 ± 2 ($n = 2$)	0.21 ± 0.05
W281C	5.3	30	*cis* and *trans*	−56 ± 12 ($n = 4$)	33 ± 9 ($n = 2$)	14 ± 5 ($n = 3$)	0.30 ± 0.10
A282C	6.2	30	*cis* and *trans*	−45 ± 7 ($n = 4$)	30 ± 10 ($n = 3$)	2.8 ± 0.3 ($n = 2$)	0.09 ± 0.03
V283C	6.2	60	*cis*	−90 ± 4 ($n = 4$)[a]	2.6 ± 0.9 ($n = 4$)	NE ($n = 2$)	0
N284C	5.3	60	*cis*	−77 ± 3 ($n = 2$)	7.2 ± 0.4 ($n = 2$)	0.66 ± 0.12 ($n = 2$)	0.08 ± 0.01
Q287C	6.2	60	*cis*	−30 ± 3 ($n = 4$)	3.0 ± 0.6 ($n = 3$)	NE ($n = 2$)	0
V288C	6.2	60	*cis*	−37 ± 4 ($n = 5$)	4.0 ± 0.9 ($n = 5$)	NE ($n = 2$)	0

The percent conductance change, reaction rates k_{cis} and k_{trans} (Eq. 1), and relative accessibility value *f* (Eq. 2) are given as mean ± standard deviation, with *n* being the number of experiments. All experiments used 1 M KCl buffer solutions with *cis* pH as specified and *trans* pH 7.2. The "MTS-ET side" column indicates whether *cis* or *trans* experiments were used to determine the macroscopic conductance change. NE: No effect

[a] For these mutants, reaction with MTS-ET promoted channel closure, making the macroscopic conductance changes unsuitable for calculating the reaction rates (Eq. 1a); we used the single-channel conductance changes (Table 2) instead. For A276C, this effect was so pronounced that we do not consider the calculated *f* value to be reliable

Single-Channel Results

The mutants that showed a macroscopic effect of MTS-ET were also examined at the single-channel level. All 15 of these mutants showed a decrease in single-channel conductance upon reaction with MTS-ET, with the greatest effects for the mutants from N277C to N284C (Table 2). We further tested selected mutants with MTS-ACE, an uncharged reagent similar in size to MTS-ET. Mutants N277C, W281C, and N284C all showed effects of MTS-ACE on the single-channel conductance that were nearly as great as the MTS-ET effects (Table 2), supporting the idea that the mutated residues lie in a sterically restricted part of the channel. (In contrast, MTS-ACE had no effect on A274C channels, suggesting that residue 274 is in a wider part of the channel.)

We also did single-channel experiments with higher time resolution, so that we could tell whether MTS-ET reacted in the channel's open state or in the brief "flicker-closed" state described by Huynh et al. (1997). Figure 4a shows an example of a channel (N284C) reacting in the open state and Fig. 4b shows one (N283C) reacting in the flicker-closed state. The results for all the reactive mutants are shown in Table 3. (Mutants A276C, A280C, and A282C sometimes reacted via a rather variable high-conductance state; we have included these events together with the closed-state reactions.) All of the mutant channels reacted primarily in the open state, with the exception of A276C, A280C, A282C, and V283C.

Figure 5 combines data from Tables 2 and 3 to show graphically the effect of MTS-ET reaction on the single-channel conductance at positive voltages (most at 60 mV), with filled bars and open bars used for mutants that reacted in the open or closed state, respectively.

We also examined the effects of MTS-ET reaction over a range of voltages. Figure 6 shows single-channel *I–V* relations for each reactive mutant, before and after reaction. These data show that MTS-ET reaction induced current rectification for some mutant channels. Among the mutants that showed larger effects of reaction, the conductance decrease was greater at negative voltages for G268C, A274C, and N277C, and the decrease was greater at positive voltages for A280C, A282C, and N284C, with relatively little rectification for W281C channels.

Effects of MTS-ET on Ionic Selectivity

For selected mutants, we examined how the channel's ionic selectivity for K^+ versus Cl^- was affected by reaction with MTS-ET. With buffer solutions of 1 M KCl, pH 5.3 on the *cis* side and 0.1 M KCl, pH 7.2 on the *trans* side, the reversal potentials before reaction were in the range −35 to −44 mV (Table 4), roughly comparable to the range (−39 to −42 mV) that we have previously obtained for

Table 2 Percent change in single-channel conductance of mutant channels upon reaction with MTS compounds

Mutant	*cis* pH	mV	MTS and side	Single-channel conductance change (%)
G268C	5.3	60	*trans* ET	-32.0 ± 2.6 ($n = 25$)
T269C	5.3	60	*trans* ET	-13.7 ± 2.4 ($n = 32$)
V272C	5.3	60	*trans* ET	-29.8 ± 2.1 ($n = 103$)
A274C	5.3	60	*trans* ET	-33.5 ± 2.2 ($n = 49$)
"	5.3	60	*trans* ACE	No effect ($n = 2$)
G275C	6.2	60	*trans* ET	-19.4 ± 1.0 ($n = 6$)
A276C	5.3	60	*trans* ET	-33.1 ± 2.7 ($n = 18$)
N277C	5.3	120	*cis* and *trans* ET	-40 ± 4 ($n = 3$)
"	5.3	60	*trans* ACE	-34.5 ± 1.2 ($n = 2$)
Y278C	5.3	60	*trans* ET	-54.7 ± 0.9 ($n = 10$)
A280C	5.3	60	*trans* ET	-49.8 ± 0.7 ($n = 3$)
"	6.2	60	*cis* and *trans* ET	-61.9 ± 2.7 ($n = 9$)
W281C	5.3	60	*cis* and *trans* ET	-54.7 ± 1.7 ($n = 14$)
"	5.3	30-60	*trans* ACE	-40.2 ± 1.1 ($n = 2$)
A282C	6.2	60	*cis* and *trans* ET	-62 ± 5 ($n = 9$)
V283C	6.2	60	*cis* ET	-39 ± 1 ($n = 9$)
N284C	6.2	60	*cis* ET	-84.4 ± 1.1 ($n = 4$)
"	6.2	60	*cis* ACE	-72.8 ± 1.0 ($n = 2$)
Q287C	6.2	60	*cis* ET	-22.1 ± 0.3 ($n = 2$)
V288C	6.2	60	*cis* ET	-31.9 ± 0.6 ($n = 5$)

The percent conductance change is given as mean $\pm$ standard deviation, with n being the number of single-channel reactions observed. All experiments used 1 M KCl buffer solutions with *cis* pH as specified and *trans* pH 7.2

T-domain mutated in the TH6–TH7 segment (Kienker et al. 2015) and indicating moderately high selectivity for K^+ over Cl^-. Upon reaction with MTS-ET, the reversal potential shifted to substantially less negative values for N277C, Y278C, and N284C channels, and even became slightly positive for W281C channels (Table 4). This indicates diminished selectivity for K^+ for the first three, and even a slight preference for Cl^- over K^+ in the case of W281C. We also examined A274C, V283C, Q287C, and V288C channels, but found only minor effects of MTS-ET reaction on the reversal potentials. This offers further support to the idea that residues 277–284 are in a more constricted part of the channel, where attaching a positively charged group can have a greater effect on ion permeation.

Discussion

We have examined a series of cysteine mutations (residues 268–290) in and near segment TH5 of the DT T-domain in order to determine the locations of the cysteine residues in the open-channel state. In particular, we hoped to use SCAM (Karlin and Akabas 1998) to learn which residues line the channel; this could also provide information about the secondary structure of this segment in the open-channel state. An additional objective was to estimate the relative accessibility of each residue to the *cis* and *trans* solutions (Wilson and Karlin 1998; Karlin 2001; Kienker et al. 2015). Although the general orientation of the TH5 segment in the open state was not really in question, given previous results that placed residue 267 on the *trans* side and residue 291 on the *cis* side (Senzel et al. 2000), we wanted to see whether our f value analysis would confirm this orientation and also identify a channel constriction as done previously with the TH6–TH7 and TH8 segments (Kienker et al. 2015).

Identification of Channel-Lining Residues in the TH5 Segment

We applied SCAM (Karlin and Akabas 1998) to residues 268–290 of the T-domain, a segment that includes the end of TH4, the TH4–TH5 loop, TH5, and the TH5–TH5′ loop (Bennett et al. 1994). We found that 15 of the 23 mutant channels showed a decrease in single-channel conductance upon reaction with the positively charged reagent MTS-ET: G268C, T269C, V272C, A274C, G275C, A276C, N277C, Y278C, A280C, W281C, A282C, V283C, N284C, Q287C, and V288C (Table 2; Fig. 5). Greater conductance changes (-39 to -84 %) were seen for the reactive mutants from N277C through N284C, with lesser changes (-14 to -34 %) for the flanking mutants G268C-A276C

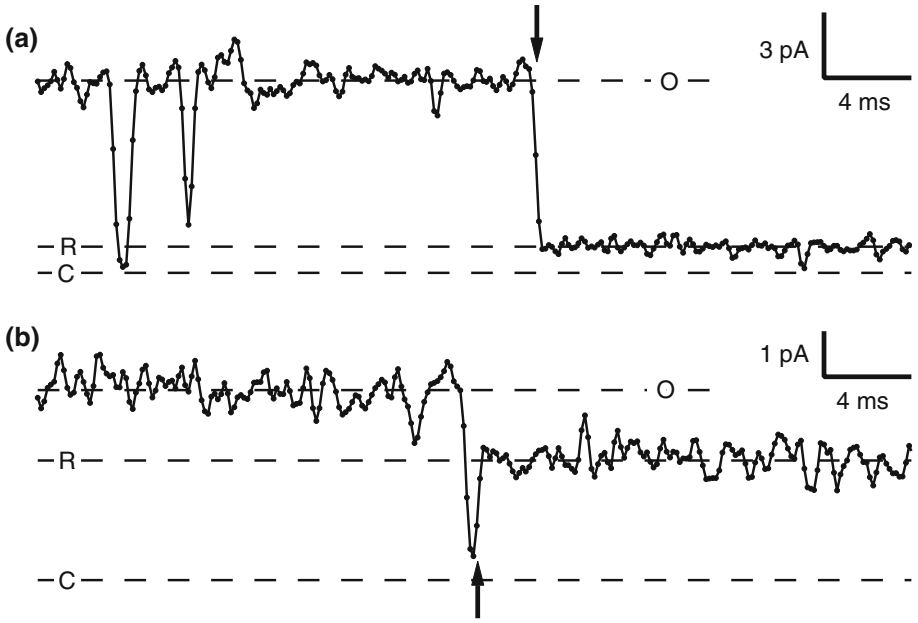

Fig. 4 Determination of the conductance state in which single T-domain mutant channels reacted with MTS-ET. Each panel shows a trace of single-channel current against time. The average closed, open, and reacted levels are shown by horizontal dashed lines labeled *C*, *O*, and *R*, respectively. **a** An N284C mutant channel reacted in the open state, 11 s after the addition of 4 mM MTS-ET to the *cis* side. **b** A V283C mutant channel reacted during a brief flicker to the closed state, 32 s after the addition of 11 mM MTS-ET to the *cis* side. The membrane potential was held at 90 mV in (**a**) and 60 mV in (**b**). The conductances of the open and reacted channels, respectively, are 98 and 13 pS in (**a**) and 70 and 44 pS in (**b**). In each panel, the reaction is marked by an *arrow*, which points down in (**a**) and up in (**b**). Both experiments used T-domain without the amino-terminal His_6-tag. At the start of each experiment, the solutions were the same as in Fig. 3, except that the *cis*-side buffer was 5 mM MES, pH 5.3. After channel formation (and before MTS-ET addition), ~5 mM HEPES, pH 7.5, was added to the *cis* side to raise the *cis* pH to 6.2. The current is drawn as small, *filled circles* connected by *lines*, with each *circle* representing a sampled data point. The sampling interval was 0.15 ms and the low-pass filtering frequency was 1000 Hz. The zero-current level was near the closed-state level

and Q287C-V288C. Reaction with the uncharged reagent MTS-ACE caused nearly as large a decrease as reaction with the comparably sized MTS-ET for mutants N277C, W281C, and N284C (Table 2), suggesting that these mutated residues might reside in a sterically constricted region of the channel. (For both reagents, N284C showed the greatest decrease.) Reaction with MTS-ET also caused large decreases in cation selectivity for N277C, Y278C, W281C, and N284C channels, with the greatest effect for W281C (Table 4).

Secondary Structure of the TH5 Segment

The pattern of reactivity given above does not immediately offer a clear indication of secondary structure, but the situation is improved when the state in which the channels reacted is taken into account. The mutants that showed a significant tendency to react in the closed state—A276C, A280C, A282C, and V283C (Table 3)—cluster together when the sequence is plotted with an α-helical periodicity (Fig. 7). Moreover, this separation of residues reacting in the closed state from those reacting in the open state extends for roughly the entire length of the TH5 helix as defined in the aqueous crystal structure, residues 275–288 (Bennett et al. 1994). We have (inappropriately) drawn all of the residues from 268 to 290 with an α-helical periodicity, but Fig. 7 gives no indication that the loops that flank the TH5 helix become helical in the open-channel state. Thus, our results are consistent with the TH5 helix remaining helical, with the N277-W281-N284 side facing the aqueous channel [as predicted by Wang and London (2009)], while the flanking loops remain loops.

Mapping the Topography of the TH5 Segment

The reaction rates of *cis*- and *trans*-side MTS-ET with TH5 segment mutant channels showed a clear division between mutants that reacted more rapidly from the *trans* side (G268C to Y278C) and those that reacted more rapidly from the *cis* side (A280C to V288C) (Table 1). In order to better quantify this trend, we plotted the relative accessibility value, f (Eq. 2), for 14 of the reactive mutants (Fig. 8). This graph shows that the transition from *trans*-exposed ($f \approx 1$) to *cis*-exposed ($f \approx 0$) residues (for

Table 3 State in which mutant channels reacted with MTS-ET

Mutant	*cis* pH	mV	MTS-ET side	Number in open state	Number in closed and/or high-conductance states
G268C	5.3	60	*trans*	13	1
T269C	5.3	60	*trans*	13	2
V272C	5.3	60	*trans*	30	4
A274C	5.3	60	*trans*	10	1
G275C	6.2	60	*trans*	3	0
A276C	5.3	60	*trans*	2	4
N277C	5.3	120	*trans*	2	0
“	5.3	60–120	*cis*	4	1
Y278C	5.3	60	*trans*	11	0
A280C	5.3	60	*trans*	2	1
“	6.2	60	*trans*	1	1
“	6.2	60	*cis*	1	2
W281C	5.3	60–90	*trans*	2	0
“	5.3	60	*cis*	4	0
A282C	6.2	60	*trans*	2	1
“	6.2	60	*cis*	1	1
V283C	6.2	60	*cis*	2	2
N284C	6.2	50–90	*cis*	3	0
Q287C	6.2	60	*cis*	2	0
V288C	6.2	60	*cis*	3	0

The number of single-channel reactions observed in each conductance state is given. All experiments used 1 M KCl buffer solutions with *cis* pH as specified and *trans* pH 7.2. We used a low-pass filtering frequency of 1000 Hz so that brief sojourns ($\sim$1 ms) in the flicker-closed state could be adequately resolved

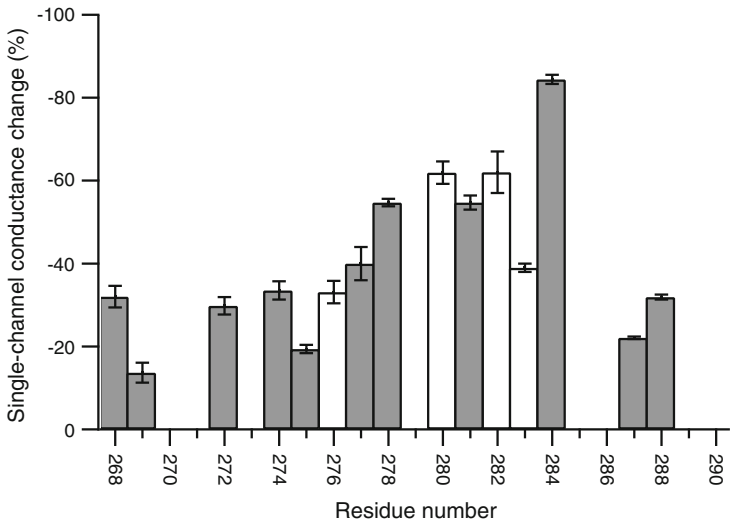

Fig. 5 Percent change in single-channel conductance of each mutant upon reaction with MTS-ET. Filled bars are used for mutants that reacted primarily in the open state and open bars for those that reacted in closed and/or high-conductance states. (Mutants without a bar did not show a reaction.) The membrane potential was held at 60 mV, except that for N277C it was held at 120 mV. Solutions had a pH gradient of either 5.3 (*cis*): 7.2 (*trans*) or 6.2 (*cis*): 7.2 (*trans*) (as described in Fig. 4); the *cis* pH is given in Table 2

mutants that reacted mainly in the open state) occurred between residues 275 and 284, with the major change in *f* between residues 278 and 281.

As an alternate method for estimating the position of the reactive site, we used a Nernst–Planck model (described in the Methods section) to fit the single-channel *I–V* data in Fig. 6. The basic idea is that reaction with MTS-ET adds a positive potential whose peak is at the reactive site, and that the asymmetry of this potential in the channel gives rise to the asymmetry in the *I–V* curve of the reacted channel. The fitted model parameters for each mutant are given in Table 5. We are mainly concerned with the fractional distance parameter, ϕ, which can range from $\phi = 0$ for a site at the *cis* end of the channel to $\phi = 1$ for a site at

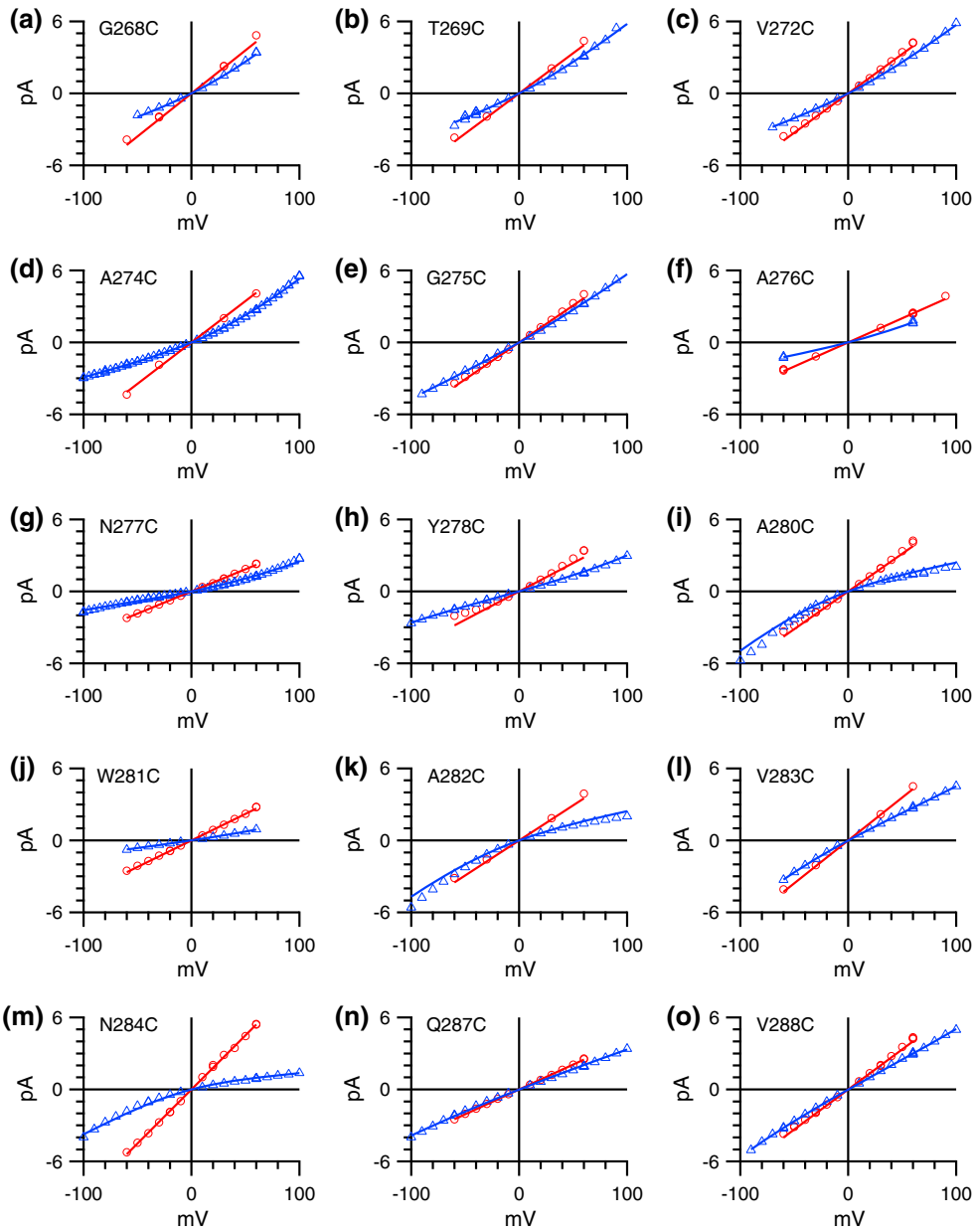

Fig. 6 Effect of MTS-ET reaction on the single-channel *I–V* relation for each mutant channel. Each panel shows current against voltage for the unreacted (*red circles*) and reacted (*blue triangles*) channel. Each experiment used a mutant T-domain without the amino-terminal His_6-tag, in order to facilitate measurements at negative voltages. Solutions had a pH gradient of 6.2 (*cis*): 7.2 (*trans*) (as described in Fig. 4). Each data set was fitted with the Nernst–Planck model as described in the Methods section. (See Table 5 for the fitted parameter values.) A slightly different procedure was used in panel (**f**), due to the fast closing of A276C channels after reaction with MTS-ET: the *cis* pH was 5.3 instead of 6.2. MTS-ET (70 μM to 11 mM) was added to the *trans* side for panels (**a**–**h**) and to the *cis* side for panels (**i**–**o**). The plotted data are from individual channels, but all experiments were performed at least twice with similar results

the *trans* end. For comparison with *f* in Fig. 8, we have also plotted ϕ (as "×" symbols). The ϕ parameter gives a very similar result to that of *f*, with the transition from *trans*- to *cis*-side positions occurring between residues 275 and 284. (We do not want to make too much of the precise values of ϕ, on account of the oversimplified geometry of the model, but the overall trend from *trans* to *cis* is clear.)

If the T-domain channel had a uniform cross-sectional area, then the *f* and ϕ values discussed above could be interpreted straightforwardly as measures of distance through the channel. As discussed below, however, we think that there is a constriction in the channel. Although it is beyond the scope of this article to model the channel's shape quantitatively, we can consider the extreme case in which essentially all of the channel's resistance comes from the constricted region. In this case, *f* and ϕ would measure progress through the constriction, rather than through the whole channel, and mutated residues in the *cis* and *trans* vestibules of the channel would give *f* (or ϕ) values of 0 and 1, respectively.

Table 4 Change in ionic selectivity of mutant channels upon reaction with MTS-ET

Mutant	MTS-ET side	V_r before (mV)	V_r after (mV)	Change in V_r (mV)
N277C	*trans*	-35.4 ± 1.1 ($n = 3$)	-23 ± 4 ($n = 4$)	11 ± 3 ($n = 3$)
Y278C	*trans*	-40.2 ± 0.2 ($n = 2$)	-12.4 ± 0.2 ($n = 2$)	27.8 ± 0.4 ($n = 2$)
W281C	*cis*	-37.4 ± 0.8 ($n = 2$)	4.5 ± 0.1 ($n = 2$)	41.8 ± 1.0 ($n = 2$)
N284C	*cis*	-43.7 ± 0.2 ($n = 3$)	-31 ± 2 ($n = 3$)	13 ± 2 ($n = 3$)

Reversal potentials V_r are given as mean $\pm$ standard deviation, with n being the number of experiments. All experiments used buffer solutions of 1 M KCl, pH 5.3 on the *cis* side and 0.1 M KCl, pH 7.2 on the *trans* side. The initial negative values of V_r indicate selectivity for K^+ over Cl^-. The positive changes in V_r upon reaction indicate decreased selectivity for K^+, or even a slight preference for Cl^- in the case of W281C. In addition, we tested mutant channels A274C (with *cis* pH 5.3 and *trans* MTS-ET) and V283C, Q287C, and V288C (with the *cis* pH raised to 6.2 and *cis* MTS-ET), but reaction had only minor effects on the reversal potential

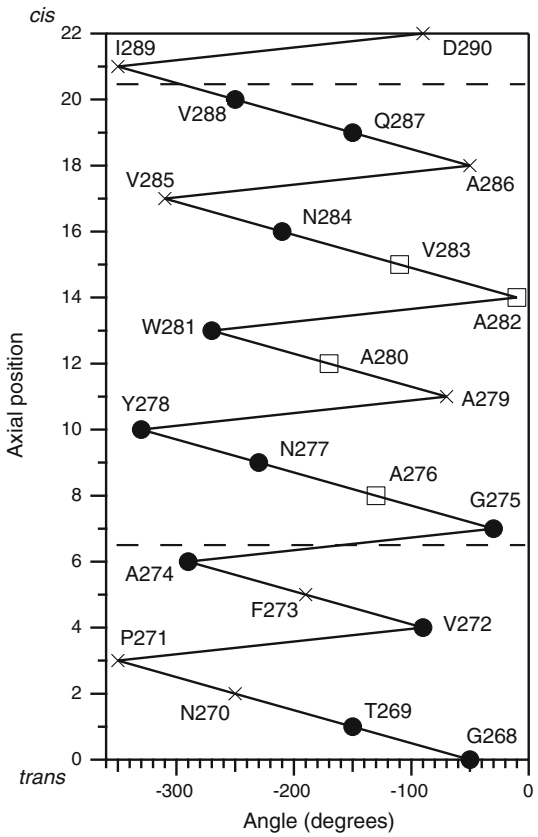

Fig. 7 Helical-net diagram (Dunnill 1968) showing the pattern of reaction in different conductance states of mutant channels. The diagram represents an α helix as a cylinder that is cut on its side and flattened out to make a *rectangle*. The entire segment from residue 268–290 is drawn with an α-helical periodicity, although only residues 275–288 form the TH5 helix in the aqueous crystal structure (Bennett et al. 1994). (This shorter segment is delimited by the *horizontal dashed lines* in the figure.) *Filled circles* represent mutant channels that reacted primarily in the open state, *open squares* those that reacted in closed and/or high-conductance states, and × symbols those that did not show a reaction. Positions that reacted in the closed state are clustered together in the diagram, supporting the idea that TH5 remains α-helical in the open-channel state

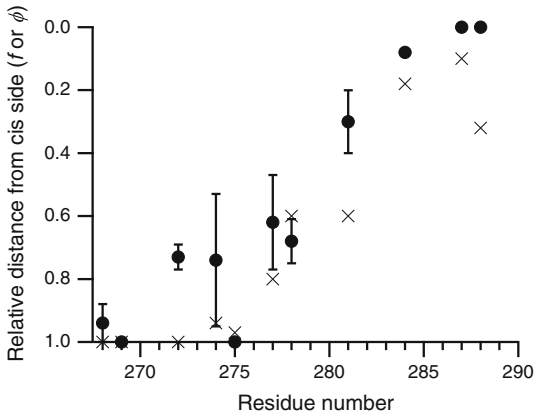

Fig. 8 Plot of the relative accessibility value, f, and fractional distance parameter, ϕ, against residue number in the TH5 segment. Only mutants that reacted primarily in the open-channel state (Table 3) are included. The f values (represented by *filled circles*) are taken from Table 1; *error bars* smaller than the symbols are omitted. Values of ϕ, the parameter indicating the position of the peak of the potential barrier in the Nernst–Planck model, are taken from Table 5 and are plotted as × symbols

Location of the TH5 Segment Relative to the Other Channel Segments

We previously obtained evidence for a constricted region in the T-domain channel, formed, at least in part, by the TH6–TH7 segment (Kienker et al. 2015). This conclusion was based primarily on the abrupt changes in the relative accessibility value, f; for instance, mutant L304C gave $f = 0$, while L307C gave $f = 0.95$. As a three-residue stretch of polypeptide is not long enough to span a lipid bilayer, this segment must occupy a small part of the total channel length. Reaction with MTS-ET also caused large changes in ionic selectivity for mutants S305C and S312C, suggesting that the mutated residues may be near the constriction. Similarly, in the TH8 segment, mutant A334C

Table 5 Fitted parameters of the Nernst–Planck model

Mutant	g (pS)	ϕ	H (mV)	$P_{K/Cl}$
G268C	72	1.00	25	20
T269C	67	1.00	21	20
V272C	66	1.00	19	20
A274C	69	0.94	34	20
G275C	61	0.97	10	20
A276C	40	0.82	36	10
N277C	37	0.80	40	20
Y278C	47	0.60	35	20
A280C	63	0.00	35	20
W281C	44	0.60	74	20
A282C	58	0.00	32	20
V283C	72	0.19	21	20
N284C	90	0.18	108	20
N284C[a]	41	0.00	31	18.5
Q287C	41	0.10	9	20
V288C	67	0.32	16	20

The parameters were obtained by fitting the Nernst–Planck model described in the Methods section to the single-channel *I–V* data in Fig. 6. In most cases, the pertinent experiments used solutions of pH 6.2 (*cis*) versus 7.2 (*trans*) and the permeability ratio $P_{K/Cl}$ was set to 20; for A276C, the *cis* pH was 5.3 and $P_{K/Cl}$ was set to 10

[a] This alternate parameter set for N284C was obtained by choosing $P_{K/Cl}$ and H to match the experimental reversal potentials (before and after MTS-ET reaction) given in Table 4; then, g and ϕ were fitted to the *I–V* data for the reacted channel in Fig. 6m

gave $f = 0.23$, while L338C gave $f = 0.95$, indicating that the mutated residues, separated by one turn of an α helix, were located respectively on the *cis* and *trans* sides of the constriction.

The f values that we have measured in the TH5 segment also showed a big change over a relatively short part of the segment, from $f = 0.08$ for N284C to $f = 1$ for G275C (Fig. 8; Table 1). The main change occurred between W281C ($f = 0.30$) and Y278C ($f = 0.68$). This change in f is not quite as abrupt as that seen in the TH6–TH7 and TH8 segments, but it would seem that residues 278 and 281, separated by one turn of an α helix, lie on opposite sides of the constriction. (Given the shortness of the TH5 helix relative to the membrane thickness, perhaps it can oscillate normal to the membrane; this would tend to shift the f values closer to 0.5, as compared with a static structure.) This information allows us to align the TH5 segment with the other known membrane segments of the T-domain channel (Fig. 9). Residues are color-coded, with red, yellow, blue, and green representing increasing values of f. [Values for the TH6–TH7 and TH8–TH9 segments are taken from Kienker et al. (2015).] It can be seen that there is a rough correlation between f and the vertical position in the figure. Note that residue G268 is actually part of the TH4 helix, so the curve that we have drawn connecting the two is not to be taken literally.

Selectivity of the channel: model versus reality

The parameters of the Nernst–Planck model (Table 5) used to fit the data in Fig. 6 were derived from experiments that had 1 M KCl on both sides of the membrane, without using any information about the ionic selectivity of the channels, other than the permeability ratio, $P_{K/Cl}$, of the wild-type (unreacted) channel. We compared the reversal potentials of mutant channels reacted with MTS-ET (Table 4) with the values calculated from the model parameters. (We used KCl activities in place of concentrations in Eq. 6.) The agreement was reasonably good for N277C ($V_r = -27$ mV calculated versus −23 mV experimental) and W281C (−2 vs. 4 mV); for Y278C (−30 vs. −12 mV), the discrepancy could be corrected by using a lower value for $P_{K/Cl}$ (12) and a higher value for H (48 mV). The greatest disagreement came with N284C (23 vs. −31 mV), on account of the large barrier height, H, needed to cause the great decrease in conductance upon reaction. An alternative approach in this case is to allow for the possibility that MTS-ET reaction lowers the conductance by both steric and electrostatic effects. [This is supported by the large conductance decrease upon reaction with the uncharged reagent, MTS-ACE (Table 2).] If we allow the scaling parameter, g, to be about twofold smaller for the reacted channel than for the unreacted channel, then we obtain an

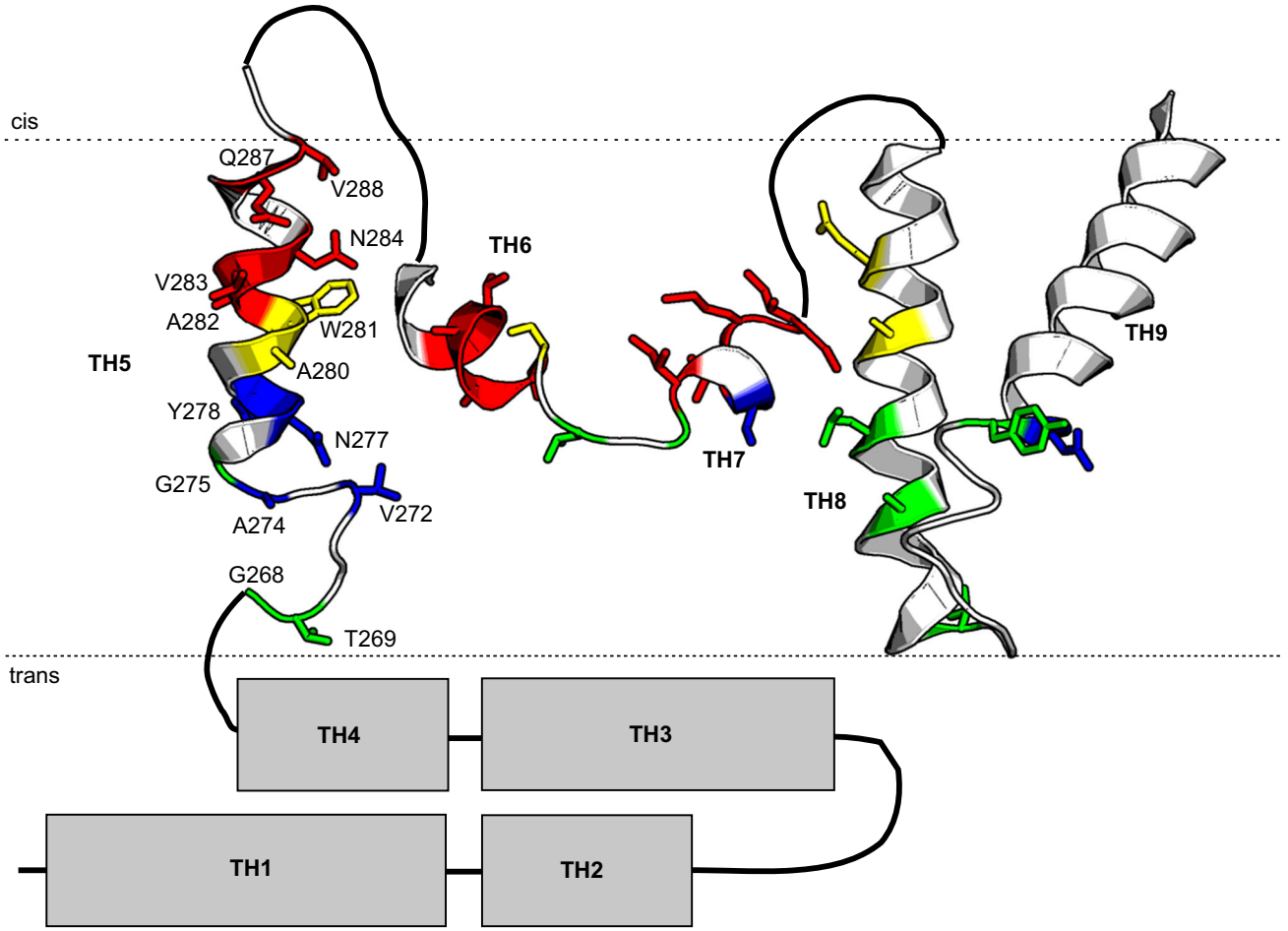

Fig. 9 Schematic model of the T-domain in the open-channel state, showing the approximate vertical alignment of the TH5, TH6–TH7, and TH8–TH9 segments. *Side chains* are shown as stick figures for all residues for which the relative accessibility value, *f*, was determined. These residues are colored *red*, *yellow*, *blue*, or *green* to represent *f* values of 0.0–0.1, 0.2–0.4, 0.6–0.8, and 0.9–1.0, respectively. There is a rough correlation between *f* and the vertical position in the figure. Residues 268–290, 297–317, and 326–376 (which roughly correspond to segments TH5, TH6–TH7, and TH8–TH9, respectively) were excerpted from the aqueous crystal structure of whole DT (Bennett et al. 1994), available from the Protein Data Bank (Berman et al. 2000) as 1DDT.pdb, reoriented as needed, and displayed using PyMOL (1.7.2.1). The polypeptide backbone is represented as a ribbon in α-helical segments and as a narrow tube in loop regions. Solid black curves represent loops that connect the segments. The pair of *horizontal dotted lines* indicates the approximate boundaries of the membrane hydrocarbon region. Note that the loop between TH4 and TH5 is not drawn accurately, as residue G268 is actually at the end of TH4. The *f* values for the TH5 segment are from this study, whereas those for the TH6–TH7 and TH8–TH9 segments are taken from Kienker et al. (2015)

alternate parameter set, with which the model can fit both the conductance and selectivity data for N284C mutant channels (Table 5).

The Channel Constriction

All of our experiments placed the channel constriction between residues N278 and N284 of the TH5 segment. Thus, (1) the relative kinetics of reaction with *cis* or *trans* MTS-ET, and hence the relative accessibility value, *f*, placed the constriction between residues Y278 and W281 (Fig. 8). (2) The greatest decreases in single-channel conductance upon reaction with MTS-ET and MTS-ACE occurred for N284C channels (Table 2); these were comparable to the largest conductance decreases seen for channels mutated in the TH6–TH7 (Kienker et al. 2015) and TH8–TH9 (Huynh et al. 1997) segments. (3) The greatest change in ionic selectivity upon reaction with MTS-ET occurred for W281C channels (Table 4), with the change in reversal potential being greater than any seen for channels mutated in the TH6–TH7 segment (Kienker et al. 2015). Finally, (4) analysis of the current rectification caused by reaction with MTS-ET put residue Y278 or W281 at the midpoint, where the reacted channel's *I–V* curve is fairly symmetric with respect to the voltage (Fig. 6). It is tempting to speculate that these two

hydrophobic residues located at the constriction of the T-domain channel play a similar role in the translocation of the catalytic domain of DT as the phenylalanine-clamp of the anthrax toxin channel (Krantz et al. 2005) plays in the translocation of the catalytic components of that toxin.

A possible concern is that some of the mutations in the vicinity of the constriction produced an abnormal single-channel conductance, when compared with that of wild-type channels. More specifically, N277C and W281C channels (as well as Q287C, not in the constriction) had reduced conductances. Given that the mutations replaced a larger side chain with a smaller one, this cannot easily be accounted for as a simple, local change in the channel, and may indicate a more large-scale change in the channel structure. It is possible that N284C channels did show such a local change in channel structure; although we counted them as normal in conductance, they were at the high end of the range (50 pS).

What Makes the Channel?

As we have long noted, it is puzzling how a large-diameter channel (Hoch et al. 1985) can be formed by a monomer of T-domain (Gordon and Finkelstein 2001) using only three transmembrane segments, TH5, TH8, and TH9 (Senzel et al. 2000). A SCAM study of the TH8–TH9 hairpin showed that TH8 and the TH8–TH9 loop lined the channel, but identified only two residues (Y358 and N359) at the amino-terminal end of TH9 as lining the channel (Huynh et al. 1997). This was surprising, given that an earlier spin-labeling study indicated that TH9 is a transmembrane helix with its full length located at a lipid/water interface (Oh et al. 1996). In light of this, the results of the present study, showing that the TH5 segment lines the channel, were not a foregone conclusion, even though TH5 had already been identified as a transmembrane segment (Senzel et al. 2000). One might have hoped that identifying two additional channel-lining segments, TH6 and TH7, would have helped to solve the puzzle of how to construct the channel, but these segments occupy only a small portion of the channel length, so they do not really solve the problem (Kienker et al. 2015).

One might ask whether we have identified all of the channel-lining segments of the T-domain. In particular, given that G268C channels showed a fairly large effect (at negative voltages) of reaction with MTS-ET (Fig. 6a), it seems possible that we have not reached the end of the channel on the *trans* side. This raises the question of whether the TH1–TH4 segments are really separate from the channel, as drawn in Fig. 9, or if some of them could be channel-lining segments. This seems unlikely, given that T-domain mutants biotinylated at residue 235 (in the TH2–TH3 loop), 261 or 267 (in the TH4 helix), or in the amino-terminal His_6-tag, were able to bind *trans* streptavidin, as indicated by a change in channel behavior (Senzel et al. 1998, 2000). Unless the *trans*-side vestibule of the channel is wide enough to admit a substantial part of the streptavidin tetramer ($\sim$50 Å diameter), it is hard to see how these residues could be located a significant distance into the membrane. The data do not rule out the possibility of a TH1–TH2 hairpin inserting partway through the membrane from the *trans* side, although the abundance of charged residues in these helices ($\geq$40 %; Greenfield et al. 1983; Bennett et al. 1994) makes this seem unlikely. Another argument against the involvement of TH1–TH4 in the T-domain channel is that residues 203–262 (from near the start of TH1 to near the start of TH4) could be deleted (in a construct with the C-domain attached) without greatly affecting the channel properties (Silverman et al. 1994). However, that study obtained similar results when the TH5–TH7 segments were also deleted, which is not consistent with our current picture of the channel; perhaps part of the C-domain was able to take the place of the deleted segments.

The best, if somewhat desperate, explanation for how to make a large-diameter channel with an inadequate amount of protein seems to be that part of the channel is lined by lipids. This could account for earlier reports that the translocating C-domain is exposed to lipid, based on photolabeling with hydrophobic reagents (Zalman and Wisnieski 1984; Hu and Holmes 1984; Montecucco et al. 1985). It was also reported that residues on one face of the TH1 helix were so labeled (D'Silva and Lala 2000); if we suppose that translocation of the "upstream" segment of the protein begins at the amino-terminal end, then we would expect there to be a translocation intermediate that has TH1 within the membrane, although it is not obvious why this segment should be photolabeled in preference to segments TH2–TH5. Recent crystal structures indicate that channels with a minimum diameter of 7 or 16 Å can be formed by three or eight transmembrane α helices, respectively, with gaps between the helices that expose lipids to the channel; domains outside of the membrane hold the helices in place (Hattori and Gouaux 2012; Tanaka et al. 2015). (The latter diameter is for a funnel-shaped pore whose diameter at the wide end is 60 Å.) The minimum diameter estimated from permeability studies of DT or fragments containing the T-domain is somewhat greater ($\geq$18 Å, Kagan et al. 1981; 24 Å, Zalman and Wisnieski 1984; $\geq$12 Å, Hoch et al. 1985), so it is still a stretch to make such a large channel with only three transmembrane helices. Another possibility is that the inserted protein segments induce a primarily lipidic pore, as has been suggested for related proteins such as colicins and Bax (Ros and García-Sáez 2015).

Acknowledgments This work was supported by the National Institutes of Health Grant GM29210.

Compliance with Ethical Standards

Conflict of interest The authors declare that they have no conflict of interest.

Research involving human and animal rights This article does not contain any studies with human participants or animals performed by any of the authors.

References

Bennett MJ, Choe S, Eisenberg D (1994) Refined structure of dimeric diphtheria toxin at 2.0 Å resolution. Protein Sci 3:1444–1463

Berman HM, Westbrook J, Feng Z, Gilliland G, Bhat TN, Weissig H, Shindyalov IN, Bourne PE (2000) The Protein Data Bank. Nucl Acids Res 28:235–242

Chenal A, Prongidi-Fix L, Perier A, Aisenbrey C, Vernier G, Lambotte S, Haertlein M, Dauvergne M-T, Fragneto G, Bechinger B, Gillet D, Forge V, Ferrand M (2009) Deciphering membrane insertion of the diphtheria toxin T domain by specular neutron reflectometry and solid-state NMR spectroscopy. J Mol Biol 391:872–883

D'Silva PR, Lala AK (2000) Organization of diphtheria toxin in membranes. A hydrophobic photolabeling study. J Biol Chem 275:11771–11777

Donovan JJ, Simon MI, Draper RK, Montal M (1981) Diphtheria toxin forms transmembrane channels in planar lipid bilayers. P Natl Acad Sci USA 78:172–176

Dunnill P (1968) The use of helical net-diagrams to represent protein structures. Biophys J 8:865–875

Gordon M, Finkelstein A (2001) The number of subunits comprising the channel formed by the T domain of diphtheria toxin. J Gen Physiol 118:471–480

Greenfield L, Bjorn MJ, Horn G, Fong D, Buck GA, Collier RJ, Kaplan DA (1983) Nucleotide sequence of the structural gene for diphtheria toxin carried by corynebacteriophage β. P Natl Acad Sci USA 80:6853–6857

Hattori M, Gouaux E (2012) Molecular mechanism of ATP binding and ion channel activation in P2X receptors. Nature 485:207–212

Hille B (2001) Ion channels of excitable membranes. Sinauer Associates Inc, Sunderland, MA, p 451

Hoch DH, Romero-Mira M, Ehrlich BE, Finkelstein A, DasGupta BR, Simpson LL (1985) Channels formed by botulinum, tetanus, and diphtheria toxins in planar lipid bilayers: relevance to translocation of proteins across membranes. P Natl Acad Sci USA 82:1692–1696

Hu VW, Holmes RK (1984) Evidence for direct insertion of fragments A and B of diphtheria toxin into model membranes. J Biol Chem 259:12226–12233

Huynh PD, Cui C, Zhan H, Oh KJ, Collier RJ, Finkelstein A (1997) Probing the structure of the diphtheria toxin channel. Reactivity in planar lipid bilayer membranes of cysteine-substituted mutant channels with methanethiosulfonate derivatives. J Gen Physiol 110:229–242

Kagan BL, Finkelstein A, Colombini M (1981) Diphtheria toxin fragment forms large pores in phospholipid bilayer membranes. P Natl Acad Sci USA 78:4950–4954

Karlin A (2001) SCAM feels the pinch. J Gen Physiol 117:235–237

Karlin A, Akabas MH (1998) Substituted-cysteine accessibility method. Method Enzymol 293:123–145

Kienker PK, Wu Z, Finkelstein A (2015) Mapping the membrane topography of the TH6-TH7 segment of the diphtheria toxin T-domain channel. J Gen Physiol 145:107–125

Krantz BA, Melnyk RA, Zhang S, Juris SJ, Lacy DB, Wu Z, Finkelstein A, Collier RJ (2005) A phenylalanine clamp catalyzes protein translocation through the anthrax toxin pore. Science 309:777–781

Lai B, Zhao G, London E (2008) Behavior of the deeply inserted helices in diphtheria toxin T domain: helices 5, 8, and 9 interact strongly and promote pore formation, while helices 6/7 limit pore formation. Biochemistry 47:4565–4574

Montal M (1974) Formation of bimolecular membranes from lipid monolayers. Method Enzymol 32:545–554

Montecucco C, Schiavo G, Tomasi M (1985) pH-dependence of the phospholipid interaction of diphtheria-toxin fragments. Biochem J 231:123–128

Murphy JR (2011) Mechanism of diphtheria toxin catalytic domain delivery to the eukaryotic cell cytosol and the cellular factors that directly participate in the process. Toxins (Basel) 3:294–308

Oh KJ, Zhan H, Cui C, Hideg K, Collier RJ, Hubbell WL (1996) Organization of diphtheria toxin T domain in bilayers: a site-directed spin labeling study. Science 273:810–812

Oh KJ, Senzel L, Collier RJ, Finkelstein A (1999a) Translocation of the catalytic domain of diphtheria toxin across planar phospholipid bilayers by its own T domain. P Natl Acad Sci USA 96: 8467–8470

Oh KJ, Zhan H, Cui C, Altenbach C, Hubbell WL, Collier RJ (1999b) Conformation of the diphtheria toxin T domain in membranes: a site-directed spin-labeling study of the TH8 helix and TL5 loop. Biochemistry 38:10336–10343

Ros U, García-Sáez AJ (2015) More than a pore: the interplay of pore-forming proteins and lipid membranes. J Membr Biol 248:545–561

Rosconi MP, London E (2002) Topography of helices 5-7 in membrane-inserted diphtheria toxin T domain: identification and insertion boundaries of two hydrophobic sequences that do not form a stable transmembrane hairpin. J Biol Chem 277: 16517–16527

Rosconi MP, Zhao G, London E (2004) Analyzing topography of membrane-inserted diphtheria toxin T domain using BODIPY-streptavidin: at low pH, helices 8 and 9 form a transmembrane hairpin but helices 5-7 form stable nonclassical inserted segments on the cis side of the bilayer. Biochemistry 43:9127–9139

Senzel L, Huynh PD, Jakes KS, Collier RJ, Finkelstein A (1998) The diphtheria toxin channel-forming T domain translocates its own NH_2-terminal region across planar bilayers. J Gen Physiol 112: 317–324

Senzel L, Gordon M, Blaustein RO, Oh KJ, Collier RJ, Finkelstein A (2000) Topography of diphtheria toxin's T domain in the open channel state. J Gen Physiol 115:421–434

Silverman JA, Mindell JA, Zhan H, Finkelstein A, Collier RJ (1994) Structure-function relationships in diphtheria toxin channels: I. Determining a minimal channel-forming domain. J Membr Biol 137:17–28

Tanaka K, Caaveiro JMM, Morante K, González-Mañas JM, Tsumoto K (2015) Structural basis for self-assembly of a cytolytic pore lined by protein and lipid. Nat Commun 6:6337. doi:10.1038/ncomms7337

Wang J, London E (2009) The membrane topography of the diphtheria toxin T domain linked to the A chain reveals a transient transmembrane hairpin and potential translocation mechanisms. Biochemistry 48:10446–10456

Wilson GG, Karlin A (1998) The location of the gate in the acetylcholine receptor channel. Neuron 20:1269–1281

Zalman LS, Wisnieski BJ (1984) Mechanism of insertion of diphtheria toxin: peptide entry and pore size determinations. P Natl Acad Sci USA 81:3341–3345

Zhan H, Oh KJ, Shin Y-K, Hubbell WL, Collier RJ (1995) Interaction of the isolated transmembrane domain of diphtheria toxin with membranes. Biochemistry 34:4856–4863

Zhao G, London E (2005) Behavior of diphtheria toxin T domain containing substitutions that block normal membrane insertion at Pro345 and Leu307: control of deep membrane insertion and coupling between deep insertion of hydrophobic subdomains. Biochemistry 44:4488–4498